Title: Treatment with furosemide indirectly increases inhibitory transmission in the developing hippocampus

Authors: C. Peerboom[1], T. Wijne[1] and C.J. Wierenga[1,2]

Corresponding author: Corette J. Wierenga

Affiliations:

[1] Cell Biology, Neurobiology and Biophysics, Biology department, Utrecht University, 3584 CH, Utrecht, the Netherlands,

[2] Donders Institute for Brain, Cognition and Behaviour, Radboud University, 6525 AJ, Nijmegen, the Netherlands

Author contributions

C.P., and C.J.W. designed research; C.P and T.W., performed research and analyzed data; C.P., and C.J.W. wrote the paper.

Declaration of Interests

The authors declare no competing interests.

Acknowledgements

This research was supported by a TOP grant from ZonMW (#91216021) and by the Nederlandse Organisatie voor Wetenschappelijk Onderzoek (NWO; #OCENW.KLEIN.150). We thank Prof. Thomas Kuner for providing the Cre-dependent SClm construct (Boffi et al., 2018). We thank Prof. Kevin Staley for providing the SuperClomeleon$^{lox/-}$ mouse line, Dr. Stefan Berger for the CamKIIα$^{Cre/-}$ mice and Dr. Henk Karst for sharing these mice with us. We thank Dunya Selemangel for help with SuperClomeleon data analysis and René van Dorland for excellent technical support.

Abstract

During the first two postnatal weeks intraneuronal chloride concentrations in rodents gradually decrease, causing a shift from depolarizing to hyperpolarizing γ-aminobutyric acid (GABA) responses. GABAergic depolarization in the immature brain is crucial for the formation and maturation of excitatory synapses, but when GABAergic signaling becomes inhibitory it no longer promotes synapse formation. Here we examined the role of chloride transporters in developing postnatal hippocampal neurons using furosemide, an inhibitor of the chloride importer NKCC1 and chloride exporter KCC2 with reported anticonvulsant effects. We treated organotypic hippocampal cultures made from 6 to 7-day old mice with 200 µM furosemide from DIV1 to DIV8. Using perforated patch clamp recordings we observed that the GABA reversal potential was depolarized after acute furosemide application, but after a week of furosemide treatment the GABA reversal potential but was more hyperpolarized compared to control. Expression levels of the chloride cotransporters were unaffected after one week furosemide treatment. This suggests that furosemide inhibited KCC2 acutely, while prolonged treatment resulted in (additional) inhibition of NKCC1, but we cannot exclude changes in HCO_3^-. We assessed the effects of accelerating the GABA shift by furosemide treatment on inhibitory synapses onto CA1 pyramidal cells. Directly after cessation of furosemide treatment at DIV9, inhibitory synapses were not affected. However at DIV21, two weeks after ending the treatment, we found that the frequency of inhibitory currents was increased, and VGAT puncta density in *stratum Radiatum* was increased. In addition, cell capacitance of CA1 pyramidal neurons was reduced in furosemide-treated slices at DIV21 in an activity-dependent manner. Our results suggest that furosemide indirectly promotes inhibitory transmission, but the underlying mechanism remains unresolved. The furosemide-induced increase in inhibitory transmission might constitute an additional mechanism via which furosemide reduces seizure susceptibility in the epileptic brain.

39 ***Introduction***

40 γ-Aminobutyric acid (GABA) is the main inhibitory, hyperpolarizing neurotransmitter in the
41 adult brain, but during early development GABA actually depolarizes neurons. Ionotropic
42 $GABA_A$ receptors primarily conduct chloride (~70%), but also HCO_3^- ions (~30%) (Kaila et al.,
43 2014). While HCO_3^- levels remain constant, intracellular chloride levels decrease during brain
44 development (Kaila et al., 2014). This developmental decrease in chloride causes the reversal
45 potential (E_{GABA}) to gradually drop below resting membrane potential. As a result, the
46 GABAergic driving force shifts from depolarizing in immature neurons to hyperpolarizing in
47 the mature brain (Rivera et al., 1999; Hübner et al., 2001; Tyzio et al., 2007; Romo-Parra et
48 al., 2008; Kirmse et al., 2015; Tsukahara et al., 2015; Sulis Sato et al., 2017; Murata and
49 Colonnese, 2020). The decrease in chloride levels is the direct result of an increased function
50 of the chloride exporter KCC2 (K-Cl cotransporter 2) relative to the chloride importer NKCC1
51 (Na-K-2Cl cotransporter 1) (Rivera et al., 1999; Gulyás et al., 2001; Yamada et al., 2004; Dzhala
52 et al., 2005; Otsu et al., 2020). In humans, the shift in chloride transporter expression occurs
53 during the first year after birth (Dzhala et al., 2005; Sedmak et al., 2016). In rodents, the GABA
54 shifts during the first two postnatal weeks (Rivera et al., 1999; Stein et al., 2004; Tyzio et al.,
55 2007; Romo-Parra et al., 2008; Kirmse et al., 2015; Sulis Sato et al., 2017; Murata and
56 Colonnese, 2020).

57

58 Depolarizing GABA signaling plays a critical role in the formation and maturation of excitatory
59 synapses in the developing brain (Leinekugel et al., 1997; Akerman and Cline, 2006; Wang and
60 Kriegstein, 2008, 2011; Chancey et al., 2013; van Rheede et al., 2015; Oh et al., 2016).
61 However, after the first postnatal week, GABA becomes inhibitory and it no longer promotes
62 synapse formation (Salmon et al., 2020; Peerboom et al., 2023). Here we examined the role
63 of chloride transporters in developing postnatal hippocampal neurons using furosemide, a
64 well-known inhibitor of chloride transport. Low furosemide concentrations (100-1000 µM)
65 have been employed previously to block KCC2 and elevate chloride concentrations in (slice)
66 cultures (Thompson and Gahwiler, 1989; Jarolimek et al., 1999; Deeb et al., 2013; Wright et
67 al., 2017), as furosemide has a preference for inhibiting KCC2 over NKCC1 (IC_{50} ~30 µM for rat
68 NKCC1 and IC_{50}~10 µM for rat KCC2, expressed in Xenopus oocytes (Orlov et al., 2015)). In
69 addition, furosemide can inhibit α6- and α4-subunit containing $GABA_A$ receptors (Thompson

and Gahwiler, 1989; Pearce, 1993; Korpi et al., 1995), and proteins that regulate neuronal HCO_3^- levels (Halligan et al., 1991; Temperini et al., 2009; Ruusuvuori and Kaila, 2014; Uwera et al., 2015). Moreover, furosemide was shown to inhibit activity-induced swelling of epileptic brain tissue (Hochman et al., 1995; Gutschmidt et al., 1999; Hochman, 2012).

Furosemide is commonly used as a diuretic, but has anti-epileptic actions as well. A case-control study on hypertension and epilepsy showed that diuretics including furosemide protected patients with hypertension against an increased risk on seizures in later life (Hesdorffer et al., 1996). Subsequently, the antiepileptic effects of furosemide were demonstrated in several animal models (Hochman et al., 1995; Gutschmidt et al., 1999; Holtkamp et al., 2003; Barbaro et al., 2004; Viitanen et al., 2010; Hochman, 2012; Uwera et al., 2015; Chen et al., 2022). Since then, several epidemiological and experimental studies have reported anticonvulsant actions of furosemide, but because of its wide range of actions, the mechanism behind furosemide's anti-epileptic effects remains mostly unclear (Hesdorffer et al., 1996; Staley, 2002; Maa et al., 2011).

We examined the effects of 200 µM furosemide in organotypic hippocampal cultures. We observed that acute furosemide application depolarized GABA reversal potential, in line with a preferential inhibition of KCC2. In contrast, furosemide treatment from DIV1 to DIV8 resulted in hyperpolarization of the GABA reversal potential. Expression levels of the chloride-cotransporters were unaffected after furosemide-treatment. This suggests that sustained application of furosemide resulted in inhibition of NKCC1, although we cannot exclude changes in HCO_3^- levels. We assessed the consequences of the accelerated GABA shift during furosemide treatment on inhibitory transmission. We found that inhibitory synapses were not affected directly after furosemide treatment at DIV9. However at DIV21, when E_{GABA} had normalized, inhibitory currents were strongly increased in furosemide-treated slices, possibly via an increased number of inhibitory synapses in the *stratum Radiatum*. In addition, we found evidence for shrinkage of CA1 pyramidal neurons in furosemide-treated slices at DIV21. Our results suggest that furosemide may indirectly promote inhibitory transmission, which could constitute a new mechanism via which furosemide can reduce seizures in the epileptic brain.

Methods

Animals

All animal experiments were performed in compliance with the guidelines for the welfare of experimental animals issued by the Federal Government of the Netherlands and were approved by the Dutch Central Committee Animal experiments (CCD), project AVD1080020173847 and project AVD1150020184927. In this study we used male and female transgenic mice: GAD65-GFP mice (López-Bendito et al., 2004) (bred as a heterozygous line in a C57BL/6JRj background), C57BL/6JRj littermates, and SuperClomeleon (SClm) mice. The SClm mice (Herstel et al., 2022) are SuperClomeleon$^{lox/-}$ mice (Rahmati et al., 2021), a gift from Kevin Staley (Massachusetts General Hospital, Boston, MA) crossed with CamKIIα$^{Cre/-}$ mice (Tsien et al., 1996; Casanova et al., 2001a). SClm mice express the chloride sensor SClm in up to 70% of the pyramidal neurons in the hippocampus (Casanova et al., 2001b; Wang et al., 2013). GAD65-GFP mice express GFP in ∼20% of GABAergic interneurons in the CA1 region of the hippocampus (Wierenga et al., 2010). As we did not detect any differences between slices from male and female mice as well as between GAD65-GFP mice and C57BL/6JRj littermates, all data were pooled.

Organotypic hippocampal culture preparation and furosemide-treatment

Organotypic hippocampal cultures were made from P6-7 mice as described before (Hu et al., 2019; Herstel et al., 2022), based on the *Stoppini method* (Stoppini et al., 1991). Mice were decapitated and their brain was rapidly placed in ice-cold Grey's Balanced Salt Solution (GBSS; containing (in mM): 137 NaCl, 5 KCl, 1.5 $CaCl_2$, 1 $MgCl_2$, 0.3 $MgSO_4$, 0.2 KH_2PO_4 and 0.85 Na_2HPO_4) with 25 mM glucose, 12.5 mM HEPES and 1 mM kynurenic acid (pH set at 7.2, osmolarity set at ~320 mOsm, sterile filtered). 400 µm thick transverse hippocampal slices were cut with a McIlwain tissue chopper. Slices were placed on Millicell membrane inserts (Millipore) in wells containing 1 ml culture medium (consisting of 48% MEM, 25% HBSS, 25% horse serum, 25 mM glucose, and 12.5 mM HEPES, with an osmolarity of ~325 mOsm and a pH of 7.3 – 7.4). Slices were stored in an incubator (35°C with 5% CO_2). Culture medium was replaced by culture medium supplemented with 0.1% dimethyl sulfoxide (DMSO, Sigma-Aldrich) or 200 µM furosemide (furosemide, Merck, in 0.1 % DMSO). In addition, a small drop

132 of medium supplemented with DMSO or furosemide was carefully placed on top of the slices.
133 In this way, cultures were treated 3 times per week until DIV8. From DIV8 onwards, cultures
134 received normal culture medium 3 times per week. Experiments were performed at day in
135 vitro 1-3 (DIV2), 8-10 (DIV9) or 20-22 (DIV21). Please note that perforated patch experiments
136 at DIV9 were performed 1 to 55 hr after cessation of the furosemide treatment. E_{GABA} did not
137 correlate with hours after treatment and was not affected by addition of furosemide to the
138 ACSF during the perforated patch recording.
139
140 *Electrophysiology and analysis*
141 Organotypic cultures were transferred to a recording chamber and continuously perfused
142 with carbonated (95% O_2, 5% CO_2) artificial cerebrospinal fluid (ACSF, in mM: 126 NaCl, 3 KCl,
143 2.5 $CaCl_2$, 1.3 $MgCl_2$, 26 $NaHCO_3$, 1.25 NaH_2PO_4, 20 glucose; with an osmolarity of ~310 mOsm)
144 at a rate of approximately 1 ml/min. Bath temperature was maintained at 29-32°C.
145 Recordings were acquired using an MultiClamp 700B amplifier (Molecular Devices), filtered
146 with a 3 kHz Bessel filter and stored using pClamp10 software. For acute application, ACSF
147 containing 0.1% DMSO or 200 µM furosemide (dissolved in 0.1% DMSO) was bath applied for
148 5 minutes.
149 Perforated patch clamp recordings were performed in CA1 pyramidal neurons. Recording
150 pipettes with resistances of 2-4 MΩ were pulled from borosilicate glass capillaries (World
151 Precision Instruments). The pipette tip was filled with gramicidin-free KCl solution (140 mM
152 KCl and 10 mM HEPES, pH adjusted to 7.2 with KOH, and osmolarity 285 mOsm/l) and then
153 backfilled with solution containing gramicidin (60 µg/ml, Sigma). Neurons were held at -65
154 mV and the access resistance of the perforated cells was monitored constantly before and
155 during recordings by a 5 mV seal test. An access resistance of 50 MΩ was considered
156 acceptable to start recording. Recordings were excluded if the resting membrane potential
157 exceeded -50 mV or if the series resistance after the recording deviated more than 30% from
158 its original value. $GABA_A$ currents were induced by upon local application of 50 µM muscimol
159 dissolved in HEPES-ACSF (containing in mM: 135 NaCl, 3 KCl, 2.5 $CaCl_2$, 1.3 $MgCl_2$, 1.25
160 $Na_2H_2PO_4$, 20 Glucose, and 10 HEPES) every 30 sec using a Picospritzer II. Muscimol responses
161 were recorded in the presence of 1 µM TTX (Abcam) at holding potentials between -100 mV
162 and -30 mV in 10 mV steps. We plotted response amplitude as a function of holding potential
163 and calculated the chloride reversal potential from the intersection of the linear current-

164 voltage curve with the x-axis. To assess the size of $GABA_A$ currents independent of holding
165 and reversal potential, we calculated the slope of the current-voltage-plot.
166
167 For recordings of spontaneous inhibitory postsynaptic currents (sIPSCs) and miniature
168 inhibitory currents (mIPSCs) we performed whole-cell patch clamp recordings from CA1
169 pyramidal neurons using borosilicate glass pipettes with resistances of 3-6 MΩ. Pipettes were
170 filled with a KCl-based internal solution (containing in mM: 70 K-gluconate, 70 KCl, 0.5
171 ethyleneglycol- bis(β-aminoethyl)-N,N,N',N'-tetraacetic Acid (EGTA), 4 Na_2phosphocreatine,
172 4 MgATP, 0.4 NaGTP and 10 HEPES; pH adjusted to 7.2 with KOH) and ACSF was supplemented
173 with 20 µM DNQX (Tocris) and 50 µM DL-APV (Tocris). For recordings of miniature IPSCs
174 (mIPSCs), 1 µM TTX (Abcam) was also added to the ACSF. sIPSCs and mIPSCs were recorded
175 for 6 minutes. For wash in experiments, an sIPSC baseline was recorded for 6 minutes and
176 compared to sIPSCs after 20 minutes wash in of 1 µM TTX (Abcam), 0.2 µM K252a (Tocris), 5
177 µM AM251 (Sigma) or 1 µM agatoxin-IVA (smartox-biotech), again for 6 minutes. Membrane
178 capacitance and series resistance were monitored during the recordings by a 5 mV seal test.
179 Cells were discarded if series resistance was above 35 MΩ or if the resting membrane
180 potential exceeded -50 mV or if the series resistance after the recording deviated more than
181 30% from its original value.
182
183 All data were blinded before analysis. Events were selected using a template in Clampfit10
184 software. Further analysis was performed using custom-written MATLAB scripts. Rise time of
185 sIPSCs was determined as the time between 10% and 90% of the peak value. The decay tau
186 was fitted with a single exponential function. Only events with a goodness of fit $R^2 \geq 0.75$ were
187 included.
188
189 *Two-photon SuperClomeleon imaging and analysis*
190 We performed two-photon chloride imaging in CA1 pyramidal cells using the SuperClomeleon
191 sensor (Grimley et al., 2013) in cultured slices from SClm mice (Herstel et al., 2022). The SClm
192 sensor consists of Cerulean (a CFP mutant) and Topaz (a YFP mutant) joined by a flexible
193 linker. In the absence of chloride, Fluorescence Resonance Energy Transfer (FRET) occurs from
194 the CFP donor to the YFP acceptor. Chloride binding to YFP increases the distance between
195 the fluorophores and decreases FRET (Grimley et al., 2013).

196

197 At the recording day, slices were transferred to a recording chamber and continuously
198 perfused with carbonated (95% O_2, 5% CO_2) ACSF supplemented with 1 mM Trolox, at a rate
199 of approximately 1 ml/min. Bath temperature was monitored and maintained at 30-32 °C.
200 Two-photon imaging of CA1 pyramidal neurons or VGAT-positive interneurons in the CA1 area
201 of the hippocampus was performed using a customized two-photon laser scanning
202 microscope (Femto3D-RC, Femtonics, Budapest, Hungary) with a Ti-Sapphire femtosecond
203 pulsed laser (MaiTai HP, Spectra-Physics) and a 60x water immersion objective (Nikon NIR
204 Apochromat; NA 1.0) The CFP donor was excited at 840 nm. The emission light was split using
205 a dichroic beam splitter at 505 nm and detected using two GaAsP photomultiplier tubes. We
206 collected fluorescence emission of Cerulean/CFP (485 ± 15 nm) and Topaz/YFP (535 ± 15 nm)
207 in parallel. Of each slice from SClm mice, 2-5 image stacks were acquired in different fields of
208 view. The resolution was 8.1 pixels/µm (1024x1024 pixels, 126x126 µm) with 1 µm z-steps.
209

210 Image analysis was performed using ImageJ software, as described before (Herstel et al.,
211 2022). We manually determined regions of interest (ROIs) around individual neuron somata.
212 To select a representative cell population in SClm slices, in each image z-stack we selected
213 four z-planes at comparable depths in which three pyramidal cells were identified that varied
214 in CFP brightness (bright, middle and dark). We subtracted the mean fluorescence intensity
215 of the background in the same image plane before calculating the fluorescence ratio of CFP
216 and YFP. We limited our analysis to cells which were located within 450 pixels from the center
217 of the image, as FRET ratios showed slight aberrations at the edge of our images. We excluded
218 cells with a FRET ratio < 0.5 or > 1.6 to avoid unhealthy cells.
219

220 *Protein extraction and Western Blot analysis*

221 Organotypic hippocampal cultures were washed in cold PBS and subsequently lysed in cold
222 protein extraction buffer containing: 150 mM NaCl, 10 mM EDTA 10 mM HEPES, 1% Triton-
223 X100 and 1x protease and 1x phosphatase inhibitors cocktails (Complete Mini EDTA-free and
224 phosSTOP, Roche). Lysates were cleared of debris by centrifugation (14,000 rpm, 1 min, 4°C)
225 and measured for protein concentration before storage at −20°C until use. Lysates were
226 denatured by adding loading buffer and heating to 95°C for 5 min. For each sample an equal
227 mass of proteins was resolved on 4–15 % polyacrylamide gel (Bio-Rad). The proteins were

228 then transferred (300 mA, 3h) onto ethanol-activated Immobilon-P PVDF membrane
229 (Millipore) before blocking with 3% Bovine Serum Albumin in Tris- buffered saline-Tween
230 (TBST, 20 mM Tris, 150 mM NaCl, 0.1% Tween-20) for 1 h. Primary antibodies used in this
231 study were: mouse anti-NKCC1 (T4, Developmental Studies Hybridoma Bank, 1:1000), rabbit
232 anti-KCC2 (07-432, Merck, 1:1000) and s940-pKCC2 (p1551-940, LuBioSciences, 1:1000),
233 mouse anti-tubulin (T-5168, Sigma, 1:10000). Primary antibodies were diluted in blocking
234 buffer and incubated with the blots overnight at 4 °C under gentle rotation. The membrane
235 was washed 3 times 15 minutes with TBST before a 1h incubation of horseradish peroxidase
236 (HRP)-conjugated antibodies (P0447 goat anti-mouse IgG HRP, Dako, 1:2500 or P0399 swine
237 anti-rabbit IgG HRP, Dako, 1:2500), and washed 3 times 15 minutes in TBST again before
238 chemiluminescence detection. For chemiluminescence detection, blots were incubated with
239 Enhanced luminol-based Chemiluminescence substrate (Promega), and the exposure was
240 captured using the ImageQuant 800 system (Amersham). Images were analyzed in ImageJ, by
241 drawing rectangular boxes around each band and measuring average intensities. Protein
242 levels were normalized to the Tubulin loading controls.
243
244 *Immunohistochemistry, confocal microscopy and analysis*
245 Slices were fixed 4 % paraformaldehyde solution in PBS for 30 minutes at room temperature.
246 After washing slices in phosphate buffered saline (PBS), they were permeabilized for 15
247 minutes in 0.5 % Triton X-100 in PBS for 15 minutes, followed by 1 hour in a blocking solution
248 consisting of 10 % normal goat serum and 0.2 % Triton X-100 in PBS. Slices were incubated in
249 primary antibody solution at 4 °C overnight. The following primary antibodies were used:
250 rabbit polyclonal anti-KCC2 (07-432, Merck, 1:1000), rabbit anti-VGAT (131003, Synaptic
251 Systems, 1:1000), guinea pig anti-VGLUT (AB5905, Merck, 1:1000), mouse anti-NeuN
252 (MAB377, Millipore, 1:500), guinea pig anti-NeuN (ABN90, Merck, 1:1000). Slices were
253 washed in PBS and incubated in secondary antibody solution for four hours at room
254 temperature. Secondary antibodies used were: goat anti-mouse Alexa Fluor 467 (Life
255 Technologies, A21236, 1:500), goat anti-rabbit Alexa Fluor 405 (A31556, Life Technologies,
256 1:500), goat anti-guinea pig Alexa Fluor 488 (A11073, Life Technologies, 1:1000) and Goat
257 anti-guineapig Alexa Fluor 568 (A11075, Life Technologies, 1:500) Goat anti-rabbit Alexa fluor
258 647 (A21245, Life Technologies, 1:500). After another PBS wash, slices were mounted in
259 Vectashield mounting medium (Vector labs).

Confocal images were taken on a Zeiss LSM-700 confocal laser scanning microscopy system with a Plan-Apochromat 40x 1.3 NA immersion objective for KCC2 staining and 63x 1.4 NA oil immersion objective for inhibitory synapse staining. KCC2 staining was imaged in two fields of view in the CA1 *sPyr* of each slice. Inhibitory synapses were imaged in the CA1 *sPyr* and *sRad* of each slice. Image stacks (1024x1024 pixels) were acquired at 6.55 pixels/µm for KCC2 staining, 10.08 pixels/µm for VGLUT/VGAT staining. Step size in z was 0.5 µm for KCC2 staining and 0.4 µm for inhibitory synapse staining.

Confocal images were blinded before analysis. For the analysis of KCC2 levels in control and furosemide-treated slices, ROIs were drawn around 5 NeuN positive cell bodies and this was repeated in 1-3 z-planes (depending on the depth of KCC2 signal) at comparable depths, to measure average KCC2 fluorescence of 5-15 neurons per image stack. For analysis of inhibitory synapses a custom-made macro was used (Ruiter et al., 2020). Briefly, three Z-planes were averaged and background was subtracted with rolling ball radius of 10 pixels. VGAT puncta were identified using watershed segmentation. PV and CB1R channels were thresholded and colocalization with VGAT puncta was analyzed.

Statistical Analyses

Statistical analysis was performed in Prism (Graphpad). Normality was tested using the D'Agostino & Pearson test. For the comparison of two groups we either used an unpaired Student's t test (UT; parametric), a Mann-Whitney test (MW; non-parametric), a paired Student's t test (PT; parametric) or a Wilcoxon signed-rank test (WSR; non-parametric). For comparison of multiple groups, a Kruskal Wallis test (KW; nonparametric) was used, followed by a Dunn's Multiple Comparison posthoc test (DMC) or a two way ANOVA (2W ANOVA; parametric), followed by a by a Sidak's Multiple Comparisons posthoc test (SMC). Data are presented as mean ± standard error of the mean. Significance is reported as *$p<0.05$; **$p\leq0.01$; ***$p\leq0.001$.

289 ***Results***

290 *Furosemide depolarizes GABA responses acutely, but hyperpolarizes GABA responses after one*
291 *week treatment.*

292 We used perforated patch recordings upon muscimol application in CA1 pyramidal neurons
293 of cultured hippocampal slices to record the reversal potential of $GABA_A$ receptor currents.
294 Acute administration of 200 µM furosemide in DIV2 slices did not affect the GABA reversal
295 potential (E_{GABA}) (Fig. 1A) or GABA driving force (GABA DF) (Fig. 1B), in agreement with a low
296 expression of KCC2 at this age (Salmon et al., 2020; Peerboom et al., 2023). At DIV21, when
297 KCC2 expression is high (Salmon et al., 2020; Peerboom et al., 2023), acute furosemide
298 application elevated E_{GABA} and GABA DF (Fig. 1C,D). This is in agreement with previous reports
299 (Thompson and Gahwiler, 1989; Jarolimek et al., 1999; Deeb et al., 2013; Wright et al., 2017)
300 and comparable with acute inhibition of KCC2 by the specific blocker VU0463271 (VU) in slices
301 at the same developmental stage (Peerboom et al., 2023).

302 We then treated cultured hippocampal slices from DIV2 to DIV8 with 200 µM furosemide.
303 Surprisingly, we observed a strong hyperpolarization of E_{GABA} and a negative shift of the GABA
304 DF at DIV9 after one week of furosemide treatment (Fig. 1E,F). Since furosemide has been
305 shown to inhibit α6- and α4-subunit containing $GABA_A$ receptors (Thompson and Gahwiler,
306 1989; Pearce, 1993; Korpi et al., 1995), we checked if $GABA_A$ receptor inhibition may have
307 interfered with our measurements of E_{GABA} and GABA DF. As a rough indication, we
308 determined the slope of the current-voltage (IV) plot to assess GABA response amplitudes
309 independently of holding potential and reversal potential. However, IV-slopes were not
310 different (MW, p=0.46), suggesting that furosemide did not have a major effect on $GABA_A$
311 receptors.

312

313 A hyperpolarizing shift in E_{GABA} suggest that furosemide treatment resulted in a reduction of
314 intraneuronal chloride or HCO_3^- levels. To directly assess intracellular chloride levels after
315 furosemide treatment, we employed the chloride sensor SuperClomeleon (SClm) (Grimley et
316 al., 2013; Boffi et al., 2018; Rahmati et al., 2021). We used slices from SClm mice in which CA1
317 pyramidal cells express the SClm sensor and we recorded FRET ratios in control and
318 furosemide-treated slices using two-photon microscopy (Herstel et al., 2022). Remarkably,

319 we did not observe a difference in SClm FRET ratios after one week of furosemide treatment
320 (Fig. 1G,H). The discrepancy between our results from perforated patch recordings and SClm
321 imaging may be due to the decreased sensitivity of the SClm sensor for low chloride levels
322 (Grimley et al., 2013; Herstel et al., 2022). Alternatively, it may reflect concomitant changes
323 in chloride and HCO_3^-, as SClm displays substantial pH-sensitivity (Grimley et al., 2013; Boffi
324 et al., 2018; Lodovichi et al., 2022). These possibilities are discussed in more detail in the
325 discussion section.

326

327 To examine if the hyperpolarizing GABA signaling after furosemide treatment was due to
328 changes in chloride cotransporter expression, we assessed total NKCC1, KCC2 or s940-pKCC2
329 protein levels in control and furosemide-treated slices using Western blots. No significant
330 changes in the levels of NKCC1, KCC2 or S940-pKCC2 were observed (Fig. 1I,J). In addition, we
331 examined KCC2 localization in treated and control slices using immunohistochemistry. We
332 used NeuN to identify individual cell bodies and we estimated KCC2 levels in somata and
333 membranes. We previously showed that we can detect a reduction in KCC2 levels after shRNA
334 using these methods (Peerboom et al., 2023). Furosemide treatment did not significantly
335 affect KCC2 levels in somata or membranes of CA1 pyramidal neurons (Fig. 1K,L). Together,
336 this indicates that furosemide treatment during DIV2 to DIV8 hyperpolarized GABA signaling
337 without changing the expression or surface levels of KCC2, nor by changing expression levels
338 of NKCC1 and S940-pKCC2. These results suggest that furosemide treatment hyperpolarized
339 E_{GABA} via inhibition of chloride transporters KCC2 and NKCC1 without altering their expression.

340

341 *Furosemide treatment does not affect inhibitory synapses at DIV9.*

342 The results above show that one week of furosemide treatment hyperpolarized E_{GABA}, thereby
343 accelerating the GABA shift. Next, we assessed the consequences of this accelerated GABA
344 shift on inhibitory transmission. We recorded spontaneous and miniature inhibitory currents
345 (sIPSCs and mIPSCs) using whole-cell voltage clamp recordings in CA1 pyramidal cells in
346 control and furosemide-treated slices at DIV9. We found that the frequency and amplitude of
347 sIPSCs were similar in control and furosemide-treated slices at DIV9 (Fig. 2A,B). There were
348 also no differences in rise and decay kinetics and the membrane capacitance (C_m) of CA1

349 pyramidal neurons (Fig. 2C-E). This indicates that GABA signaling does not directly affect the
350 development of inhibitory synapses at this developmental stage (Peerboom et al., 2023).

351

352 When recording sIPSCs, we noticed that the sIPSC frequency slightly increased by ~20% during
353 the 20 minutes of recording in both control and furosemide-treated slices (Fig. 2F,G). When
354 we washed in TTX to block neuronal activity in control slices, this 'run-up' was prevented (Fig.
355 2H), indicating that the run-up is activity dependent. However, TTX did not prevent the run-
356 up in furosemide-treated slices, suggesting that the run up had different mechanisms in
357 control and furosemide-treated slices (Fig. 2I). We considered the possibility that the activity-
358 dependent run up is due to release of activity-dependent factors, such as endocannabinoids
359 or BDNF. We assessed the contribution of the BDNF receptor TrkB by washing in TrkB
360 antagonist K252a during sIPSC recordings in control and furosemide-treated slices. We found
361 that sIPSCs were enhanced after wash in K252a, suggesting that there is ongoing suppression
362 of GABA release by BDNF in our slices at DIV9. However, there was no differential contribution
363 of BDNF between control and furosemide-treated slices (Fig. 2J). We also washed in AM251,
364 a specific antagonist of the endocannabinoid receptor CB1. We found that endocannabinoid
365 signaling does not have a prominent influence on sIPSCs, and there was no difference
366 between control and furosemide-treated slices (Fig. 2J). Blocking presynaptic P/Q calcium
367 channels with agatoxin-IVA (aga) (Goswami et al., 2012) also did not significantly alter sIPSC
368 frequency in control and furosemide-treated slices (Fig. 2J). It therefore remains unclear why
369 activity-dependent run up of sIPSCs was different in furosemide-treated slices.

370 *Inhibitory transmission is increased in furosemide-treated slices at DIV21.*

371 Two weeks after ending the treatment at DIV21, E_{GABA} and GABA DF in pyramidal neurons had
372 normalized and reached control levels (Fig. 3A,B). We previously found that a transient
373 elevation of chloride using VU treatment from DIV2 to DIV8 resulted in indirect changes in
374 inhibitory transmission at DIV21 (Peerboom et al., 2023). We therefore assessed if furosemide
375 treatment from DIV2 to DIV8 affected sIPSCs at DIV21 (Fig. 3C). There was large variability in
376 sIPSC frequency between cells, but we did not detect any significant difference between
377 furosemide-treated and control slices (Fig. 3D). We did observe a small increase in sIPSC
378 amplitude in furosemide-treated slices (Fig. 3E), while the rise and decay time of the sIPSCs

379 were not different (Fig. 3F, G). In addition, we observed that cell capacitance C_m of CA1
380 pyramidal cells was decreased in furosemide-treated slices compared to control slices (Fig.
381 3H). To assess whether the changes in inhibitory transmission were activity-dependent, we
382 also recorded mIPSCs (Fig. 3I). We observed an increased mIPSCs frequency in furosemide-
383 treated slices at DIV21, while amplitude, rise and decay time were not different from control
384 slices (Fig. 3J-M). Interestingly, a difference in membrane capacitance C_m was not detected
385 when recording mIPSCs in the presence of TTX (Fig. 3N). When we compared C_m values during
386 sIPSC and mIPSC recording we found a significant interaction (p=0.02 ; 2w ANOVA), suggesting
387 that furosemide treatment affected cell capacitance in an activity-dependent manner.

388 A change in mIPSC frequency while amplitude remain unaffected could have resulted from an
389 increase in the number of inhibitory synapses in furosemide-treated slices compared to
390 control slices at DIV21. To assess synapse numbers, we used immunohistochemistry to
391 visualize inhibitory synapses in *stratum Pyramidale (sPyr*) and *stratum Radiatum* (*sRad*) using
392 the vesicular GABA transporter VGAT. In addition, we stained for CB1 receptors (CB1R) and
393 parvalbumin (PV), to identify inhibitory synapses from specific interneuron subtypes (Fig.
394 4A,B). The density and size of VGAT puncta in the CA1 area were similar in control and
395 furosemide-treated slices at DIV9 (Fig. 4C-F) and we did not observe any differences in the
396 density of CB1R+ and PV+ VGAT puncta (Fig. 4G-I). At DIV21 however (Fig. 5A,B), we observed
397 an increased density and reduced size of VGAT puncta in the *sRad* in furosemide-treated slices
398 compared to controls (Fig. 5E,F), but not *sPyr* (Fig. 5C,D). This suggests that the number of
399 inhibitory synapses in the dendritic region was increased at DIV21 in furosemide-treated
400 slices. The density of PV- and CB1R-positive puncta were not different in furosemide-treated
401 and control slices (Fig. 5G-I), suggesting that the increase in VGAT puncta is due to an increase
402 in synapses from another interneuron subtype.

403

404 ***Discussion***

405 In this study, we used furosemide to manipulate the GABA shift in organotypic hippocampal
406 slices. Unexpectedly, we observed that treatment with furosemide from DIV1 to DIV8 had an
407 opposite effect compared to acute furosemide application. While acute application
408 depolarized the reversal potential for GABA signaling (E_{GABA}), one week furosemide treatment

409 resulted in a strong hyperpolarizing shift of E_{GABA}. This shift was not accompanied by a change
410 in SuperClomeleon (SClm) FRET ratios or chloride co-transporter expression. We observed
411 that sIPSCs were not affected by the hyperpolarization of E_{GABA} after furosemide treatment at
412 DIV9, consistent with the notion that GABA signaling in the second postnatal week no longer
413 promotes synapse formation (Wang and Kriegstein, 2011; Salmon et al., 2020; Peerboom et
414 al., 2023). However, we found that at DIV21, two weeks after ending furosemide treatment
415 and when E_{GABA} had normalized, inhibitory currents were increased. This was accompanied
416 by an increase of the density of VGAT puncta in *sRad*. In addition, we found that cell
417 capacitance was affected in furosemide-treated slices at DIV21 in an activity-dependent
418 manner. Together, these results show that accelerating the GABA shift with furosemide does
419 not directly affect the development of inhibitory synapses. However, transient furosemide
420 treatment appeared to indirectly alter cell volume regulation and increase inhibitory
421 transmission two weeks later.

422

423 *Effect of furosemide on neuronal chloride levels*

424 The depolarizing effect of acute furosemide application at DIV21 is comparable to that of
425 acute inhibition of KCC2 by specific KCC2 blocker VU0463271 (VU) in slices at the same
426 developmental stage (Peerboom et al., 2023), suggesting that acutely applied furosemide
427 merely inhibited KCC2. At the concentration used here (200 µM), furosemide is expected to
428 block both KCC2 and NKCC1 (Orlov et al., 2015). However, NKCC1 maintains chloride levels
429 only until approximately P15-21 (Romo-Parra et al., 2008; Sulis Sato et al., 2017; Salmon et
430 al., 2020). Previous studies reporting a depolarizing effect of furosemide acutely applied the
431 compound to (slice) cultures at a developmental stage equal to P14 or later (Thompson and
432 Gahwiler, 1989; Jarolimek et al., 1999; Deeb et al., 2013; Wright et al., 2017). In our slices at
433 DIV21 (prepared from P7 mice), NKCC1 may no longer directly regulate chloride levels, which
434 explains why acute furosemide application only acted via KCC2 at DIV21.

435

436 In stark contrast, furosemide treatment from DIV1 to DIV8 resulted in hyperpolarizing E_{GABA},
437 suggestive of NKCC1 block. We checked that furosemide treatment did not affect expression
438 levels of chloride transporters. If furosemide treatment indeed hyperpolarized E_{GABA} by

439 blocking NKCC1, we would expect to observe an increase in SClm FRET ratios (reflecting a
440 decrease in chloride levels) after furosemide treatment, which was not the case. However,
441 the sensitivity of the SClm sensor is reduced at chloride concentrations below ~5 mM (Grimley
442 et al., 2013; Boffi et al., 2018; Herstel et al., 2022). This raises the possibility that chloride
443 levels in our DIV9 slices are too low to detect a further decrease by furosemide treatment
444 with the SClm sensor.

445

446 *Possible effect of furosemide on pH*

447 In addition to blocking chloride transporters, furosemide may also interfere with enzymes
448 that are involved in HCO_3^- regulation (Halligan et al., 1991; Temperini et al., 2009; Uwera et
449 al., 2015). $GABA_A$ receptors are permeable for chloride and HCO_3^- ions with a permeability of
450 around 70% and 30% respectively (Kaila et al., 2014). The reversal potential of HCO_3^- (E_{HCO3})
451 is maintained by pH-regulatory proteins at around -10 mV (Kaila et al., 2014), which is much
452 more positive than the chloride reversal potential (E_{Cl}). As a result, E_{GABA} is slightly more
453 positive than E_{Cl} and the flow of chloride through $GABA_A$ receptors is accompanied by an
454 outflow of HCO_3^- (Kaila et al., 2014). The lack of change in SClm FRET ratios after furosemide
455 treatment raises the possibility that the observed hyperpolarization of E_{GABA} reflect changes
456 in intracellular HCO_3^- levels, rather than chloride. If furosemide would decrease intraneuronal
457 HCO_3^- levels, the outflow of HCO_3^- upon $GABA_A$ receptor activation would be reduced, and
458 E_{GABA} would become more negative. Previous studies have suggested that furosemide can
459 inhibit the Cl^-/HCO_3^- anion exchanger AE3 (Halligan et al., 1991; Uwera et al., 2015). AE3
460 exchanges intracellular HCO_3^- for extracellular chloride, thereby lowering intracellular pH and
461 increasing intracellular chloride concentrations in response to intracellular alkali loads
462 (Gonzalez-Islas et al., 2009; Pfeffer et al., 2009; Romero et al., 2013). Furosemide can also
463 block carbonic anhydrase (CA) (Temperini et al., 2009), which is a cytosolic enzyme that
464 mediates the conversion of HCO_3^- ($CO_2 + H_2O \rightleftarrows HCO_3^- + H^+$) to buffer intraneuronal pH after
465 alkali or acid loads (Ruusuvuori and Kaila, 2014). To our knowledge there are no studies
466 directly examining the contribution of AE3 or CA to E_{GABA}. Theoretically, inhibition of AE3 by
467 furosemide would decrease intracellular chloride levels while increasing HCO_3^-, which have
468 opposing effects on E_{GABA}. Inhibition of CA would in theory reduce the contribution of E_{HCO3} to

469 E_{GABA} and result in a negative shift of E_{GABA} towards E_{Cl}. If the hyperpolarization of E_{GABA} was
470 solely due to changing HCO_3^- levels without changing chloride, pH values would be
471 unphysiologically low. A strong decrease in pH would decrease IPSC frequency and amplitude
472 and increase rise and decay times (Mozrzymas et al., 2003; Dietrich and Morad, 2010), while
473 we observed that IPSCs were unaffected at DIV9. We therefore deem it unlikely that
474 furosemide induced large pH changes. However, a small decrease in intracellular pH would
475 decrease SClm FRET ratios (Grimley et al., 2013; Boffi et al., 2018; Lodovichi et al., 2022),
476 which may have obscured an increase in FRET ratios due to a decrease in chloride levels. We
477 therefore conclude that furosemide treatment most likely resulted in a decrease in chloride
478 levels, but our data do not exclude a subtle change in pH regulation.

479

480 *Possible effect of furosemide on cell volume regulation*

481 We observed that the membrane capacitance of CA1 pyramidal neurons was reduced in
482 furosemide-treated slices compared to control slices at DIV21 (Fig. 3H), but not at DIV9 (Fig.
483 2E). A reduction in whole cell membrane capacitance may reflect a reduction in cell size
484 (Taylor, 2012). Remarkably, neuronal capacitance was not affected when neuronal activity
485 was blocked during mIPSC recordings (compare Fig. 3H and 3N), raising the possibility that
486 the difference in membrane capacitance reflects activity-dependent cell shrinkage. Previous
487 studies have shown that furosemide inhibits activity-induced changes in the volume of
488 neuronal tissue during epilepsy (Hochman et al., 1995; Gutschmidt et al., 1999; Hochman,
489 2012). It has been shown that this effect is mainly mediated by inhibition of NKCC1 on glia
490 (Ransom et al., 1985; Hochman, 2012). Glia disperse local, activity-induced elevations in
491 potassium and chloride ions which are followed by water and result in glial swelling (Ransom
492 et al., 1985; Hochman et al., 1995; Gutschmidt et al., 1999; Hochman, 2012). Our results
493 suggest that one week treatment with furosemide indirectly affect activity-induced swelling
494 of neurons, but the mechanism remains unresolved. In interpreting our results and that of
495 previous studies, it is hard to disentangle the versatile pharmacological profile of furosemide
496 and the many roles for neuronal chloride in regulating cell volume (Jentsch and Pusch, 2018)
497 and possibly cellular excitability (Huang et al., 2012; Seja et al., 2012; Jentsch and Pusch, 2018;
498 Goutierre et al., 2019; Sinha et al., 2022; Peerboom et al., 2023).

499

500 *Furosemide-treatment indirectly increased inhibitory transmission*

501 We observed that sIPSCs were not affected by the hyperpolarization of E_{GABA} at DIV9,
502 immediately after the furosemide treatment (Fig. 2A-E). These results confirm previous
503 studies reporting that synapse formation is mostly independent from GABA signaling after the
504 first postnatal week (Wang and Kriegstein, 2011; Peerboom et al., 2023). More surprisingly,
505 we found that furosemide treatment resulted in an increase in inhibitory transmission at
506 DIV21. The amplitude of sIPSCs and the frequency of mIPSCs were strongly increased, and this
507 was associated with an increased density of inhibitory synapses in *sRad* in furosemide-treated
508 slices compared to control slices. However, one should be cautious in interpreting synaptic
509 density in the two conditions, as furosemide treatment may have induced overall cell
510 shrinkage, which would increase apparent synaptic density. To assess synaptic densities
511 independently of cell shrinkage, the density of synapses along the dendrites (Feng et al., 2021)
512 or per soma (Bijlsma et al., 2022) should be assessed.

513 In a recent study we treated slice cultures with VU, a specific blocker of the chloride exporter
514 KCC2, to delay the postnatal GABA shift and maintain a depolarizing E_{GABA} until DIV8. Similar
515 to the current results, we also observed an indirect increase in sIPSC frequency at DIV21 cells
516 (Peerboom et al., 2023). However, the mechanism seems different as mIPSC frequency and
517 synapse numbers were not affected in VU-treated slices (Peerboom et al., 2023). These
518 observations underscore the need for a better understanding of the role of chloride as an
519 intracellular messenger in developing neurons. Although the precise mechanism remains
520 obscure, our current results suggest that furosemide treatment indirectly increases inhibitory
521 transmission, which adds to its previously described anticonvulsant action.

522

523 ***References***

524 Akerman CJ, Cline HT (2006) Depolarizing GABAergic conductances regulate the balance of excitation to inhibition in the
525 developing retinotectal circuit in vivo. J Neurosci 26:5117–5130.

526 Barbaro NM, Takahashi DK, Baraban SC (2004) A potential role for astrocytes in mediating the antiepileptic actions of
527 furosemide in vitro. Neuroscience 128:655–663.

528 Bijlsma A, Omrani A, Spoelder M, Verharen JPH, Bauer L, Cornelis C, de Zwart B, van Dorland R, Vanderschuren LJMJ,
529 Wierenga CJ (2022) Social Play Behavior Is Critical for the Development of Prefrontal Inhibitory Synapses and
530 Cognitive Flexibility in Rats. J Neurosci 42:8716–8728.

531 Boffi JC, Knabbe J, Kaiser M, Kuner T (2018) KCC2-dependent steady-state intracellular chloride concentration and ph in
532 cortical layer 2/3 neurons of anesthetized and awake mice. Front Cell Neurosci 12:1–14.

533 Casanova E, Fehsenfeld S, Mantamadiotis T, Lemberger T, Greiner E, Stewart AF, Schtz G (2001a) A CamKIIα iCre BAC allows
534 brain-specific gene inactivation. Genesis 31:37–42.

535 Casanova E, Fehsenfeld S, Mantamadiotis T, Lemberger T, Greiner E, Stewart AF, Schtz G (2001b) A CamKIIα iCre BAC allows
536 brain-specific gene inactivation. Genesis 31:37–42.

537 Chancey JH, Adlaf EW, Sapp MC, Pugh PC, Wadiche JI, Overstreet-Wadiche LS (2013) GABA Depolarization Is Required for
538 Experience-Dependent Synapse Unsilencing in Adult-Born Neurons. J Neurosci 33:6614–6622.

539 Chen L, Yu J, Wan L, Wu Z, Wang G, Hu Z, Ren L, Zhou J, Qian B, Zhao X, Zhang J, Liu X (2022) Furosemide prevents
540 membrane KCC2 downregulation during convulsant stimulation in the hippocampus. IBRO Neurosci Rep 12:355–
541 365.

542 Deeb TZ, Nakamura Y, Frost GD, Davies PA, Moss SJ (2013) Disrupted Cl-homeostasis contributes to reductions in the
543 inhibitory efficacy of diazepam during hyperexcited states. Eur J Neurosci 38:2453–2467.

544 Dietrich CJ, Morad M (2010) Synaptic acidification enhances GABAA signaling. J Neurosci 30:16044–16052.

545 Dzhala VI, Talos DM, Sdrulla DA, Brumback AC, Mathews GC, Benke TA, Delpire E, Jensen FE, Staley KJ (2005) NKCC1
546 transporter facilitates seizures in the developing brain. Nat Med 11:1205–1213.

547 Feng T, Alicea C, Pham V, Kirk A, Pieraut S (2021) Experience-dependent inhibitory plasticity is mediated by CCK1 basket
548 cells in the developing dentate gyrus. J Neurosci 41:4607–4619.

549 Gonzalez-Islas C, Chub N, Wenner P (2009) NKCC1 and AE3 appear to accumulate chloride in embryonic motoneurons. J
550 Neurophysiol 101:507–518.

551 Goswami SP, Bucurenciu I, Jonas P (2012) Miniature IPSCs in hippocampal granule cells are triggered by voltage-gated Ca2+
552 channels via microdomain coupling. J Neurosci 32:14294–14304.

553 Goutierre M, Al Awabdh S, Donneger F, François E, Gomez-Dominguez D, Irinopoulou T, Menendez de la Prida L, Poncer JC
554 (2019) KCC2 Regulates Neuronal Excitability and Hippocampal Activity via Interaction with Task-3 Channels. Cell
555 Rep 28:91–103.

556 Grimley JS, Li L, Wang W, Wen L, Beese LS, Hellinga HW, Augustine GJ (2013) Visualization of Synaptic Inhibition with an
557 Optogenetic Sensor Developed by Cell-Free Protein Engineering Automation. J Neurosci 33:16297–16309.

558 Gulyás AI, Sík A, Payne JA, Kaila K, Freund TF (2001) The KCl cotransporter, KCC2, is highly expressed in the vicinity of
559 excitatory synapses in the rat hippocampus. Eur J Neurosci 13:2205–2217.

560 Gutschmidt KU, Stenkamp K, Buchheim K, Heinemann U, Meierkord H (1999) Anticonvulsant actions of furosemide in vitro.
561 Neuroscience 91:1471–1481.

562 Halligan RD, Shelat H, Kahn AM (1991) Na+-independent Cl--HCO : exchange in sarcolemmal vesicles from vascular smooth
563 muscle. Am J Physiol 260:C347-54.

564 Herstel LJ, Peerboom C, Uijtewaal S, Selemangel D, Karst H, Wierenga CJ (2022) Using SuperClomeleon to measure changes
565 in intracellular chloride during development and after early life stress. Eneuro November/D.

566 Hesdorffer DC, Hauser WA, Annegers JF, Rocca WA (1996) Severe, uncontrolled hypertension and adult-onset seizures: A
567 case- control study in Rochester, Minnesota. Epilepsia 37:736–741.

568 Hochman DW (2012) The extracellular space and epileptic activity in the adult brain: Explaining the antiepileptic effects of
569 furosemide and bumetanide. Epilepsia 53:18–25.

570 Hochman DW, Baraban SC, Owens JWM, Schwartzkroin PA (1995) Dissociation of synchronization and excitability in
571 furosemide blockade of epileptiform activity. Science 270:99–102.

572 Holtkamp M, Matzen J, Buchheim K, Walker MC, Meierkord H (2003) Furosemide terminates limbic status epilepticus in
573 freely moving rats. Epilepsia 44:1141–1144.

574 Hu HY, Kruijssen DLH, Frias CP, Rózsa B, Hoogenraad CC, Wierenga CJ (2019) Endocannabinoid Signaling Mediates Local
575 Dendritic Coordination between Excitatory and Inhibitory Synapses. Cell Rep 27:666-675.e5.

576 Huang WC, Xiao S, Huang F, Harfe BD, Jan YN, Jan LY (2012) Calcium-Activated Chloride Channels (CaCCs) Regulate Action
577 Potential and Synaptic Response in Hippocampal Neurons. Neuron 74:179–192.

578 Hübner C a, Stein V, Hermans-Borgmeyer I, Meyer T, Ballanyi K, Jentsch TJ (2001) Disruption of KCC2 reveals an essential
579 role of K-Cl cotransport already in early synaptic inhibition. Neuron 30:515–524.

580 Jarolimek W, Lewen A, Misgeld U (1999) A furosemide-sensitive K+ -Cl- cotransporter counteracts intracellular Cl-
581 accumulation and depletion in cultured rat midbrain neurons. J Neurosci 19:4695–4704.

582 Jentsch TJ, Pusch M (2018) CLC chloride channels and transporters: Structure, function, physiology, and disease. Physiol
583 Rev 98:1493–1590.

584 Kaila K, Price TJ, Payne JA, Puskarjov M, Voipio J (2014) Cation-chloride cotransporters in neuronal development, plasticity
585 and disease. Nat Rev Neurosci 15:637–654.

586 Kirmse K, Kummer M, Kovalchuk Y, Witte OW, Garaschuk O, Holthoff K (2015) GABA depolarizes immature neurons and
587 inhibits network activity in the neonatal neocortex in vivo. Nat Commun 6:1–13.

588 Korpi ER, Kuner T, Seeburg PH, Luddens H (1995) Selective antagonist for the cerebellar granule cell-specific g-aminobutyric
589 acid type A receptor. MolPharmacol 47:283–289.

590 Leinekugel X, Medina I, Khalilov I, Ben Ari Y, Khazipov R (1997) Ca 2+ Oscillations Mediated by the Synergistic Excitatory
591 Actions of GABA. Neuron 18:243–255.

592 Lodovichi C, Ratto GM, Trevelyan AJ, Arosio D (2022) Genetically encoded sensors for Chloride concentration. J Neurosci
593 Methods 368:109455.

594 Maa EH, Kahle KT, Walcott BP, Spitz MC, Staley KJ (2011) Diuretics and epilepsy: Will the past and present meet? Epilepsia
595 52:1559–1569.

596 Mozrzymas J, Zarnowska E, Pytel M, Mercik K (2003) Modulation of GABAA receptors by hydrogen ions reveals synaptic
597 GABA transient and a crucial role of the desensitization process. J Neurosci 23:7981–7992.

598 Murata Y, Colonnese MT (2020) GABAergic interneurons excite neonatal hippocampus in vivo. Sci Adv 6:1–10.

599 Oh WC, Lutzu S, Castillo PE, Kwon HB (2016) De novo synaptogenesis induced by GABA in the developing mouse cortex -
600 supplemental. Science 353:1037–1040.

601 Orlov SN, Koltsova S V, Kapilevich L V, Gusakova S V, Dulin NO (2015) NKCC1 and NKCC2: The pathogenetic role of cation-
602 chloride cotransporters in hypertension. 2:186–196.

603 Otsu Y, Donneger F, Schwartz EJ, Poncer JC (2020) Cation–chloride cotransporters and the polarity of GABA signalling in
604 mouse hippocampal parvalbumin interneurons. J Physiol 598:1–16.

605 Pearce RA (1993) Physiological evidence for two distinct GABAA responses in rat hippocampus. Neuron 10:189–200.

606 Peerboom C, Kater S De, Jonker N, Rieter M, Wijne T, Wierenga CJ (2023) Delaying the GABA shift indirectly affects
607 membrane properties in the developing hippocampus. bioRxiv.

608 Pfeffer CK, Stein V, Keating DJ, Maier H, Rinke I, Rudhard Y, Hentschke M, Rune GM, Jentsch TJ, Hubner CA (2009) NKCC1-
609 Dependent GABAergic Excitation Drives Synaptic Network Maturation during Early Hippocampal Development. J
610 Neurosci 29:3419–3430.

611 Rahmati N, Normoyle KP, Glykys J, Dzhala VI, Lillis KP, Kahle KT, Raiyyani R, Jacob T, Staley KJ (2021) Unique actions of gaba
612 arising from cytoplasmic chloride microdomains. J Neurosci 41:4967–4975.

613 Ransom B, Yamate C, Connors B (1985) Activity-dependent in rat optic nerve: a developmental study. J Neurosci 5:532–
614 535.

615 Rivera C, Voipio J, Payne J a, Ruusuvuori E, Lahtinen H, Lamsa K, Pirvola U, Saarma M, Kaila K (1999) The K+/Cl- co-
616 transporter KCC2 renders GABA hyperpolarizing during neuronal maturation. Nature 397:251–255.

617 Romero MF, Chen AP, Parker MD, Boron WF (2013) The SLC4 family of bicarbonate (HCO3-) transporters. Mol Aspects Med
618 34:159–182.

619 Romo-Parra H, Treviño M, Heinemann U, Gutiérrez R (2008) GABA actions in hippocampal area CA3 during postnatal
620 development: Differential shift from depolarizing to hyperpolarizing in somatic and dendritic compartments. J
621 Neurophysiol 99:1523–1534.

622 Ruiter M, Herstel LJ, Wierenga CJ, Ma T (2020) Reduction of Dendritic Inhibition in CA1 Pyramidal Neurons in Amyloidosis
623 Models of Early Alzheimer's Disease. J Alzheimers Dis 78:951–964.

624 Ruusuvuori E, Kaila K (2014) Carbonic Anhydrases and Brain pH in the Control of Neuronal Excitability. In: Carbonic
625 Anhydrase: Mechanism, Regulation, Links to Disease, and Industrial Applications, pp 271–290 Subcellular
626 Biochemistry. Springer International Publishing. Available at: https://doi.org/10.1007/978-94-007-7359-2_14.

627 Salmon CK, Pribiag H, Gizowski C, Farmer WT, Cameron S, Jones E V., Mahadevan V, Bourque CW, Stellwagen D, Woodin
628 MA, Murai KK (2020) Depolarizing GABA Transmission Restrains Activity-Dependent Glutamatergic Synapse
629 Formation in the Developing Hippocampal Circuit. Front Cell Neurosci 14:1–16.

630 Sedmak G, Puskarjov NJ-MM, Ulamec M, Krušlin B, Kaila K, Judaš M (2016) Developmental Expression Patterns of KCC2 and
631 Functionally Associated Molecules in the Human Brain. Cereb Cortex 27:4060–4072.

632 Seja P, Schonewille M, Spitzmaul G, Badura A, Klein I, Rudhard Y, Wisden W, Hübner CA, De Zeeuw CI, Jentsch TJ (2012)
633 Raising cytosolic Cl - in cerebellar granule cells affects their excitability and vestibulo-ocular learning. EMBO J
634 31:1217–1230.

635 Sinha AS, Wang T, Watanabe M, Hosoi Y, Sohara E, Akita T, Uchida S, Fukuda A (2022) WNK3 kinase maintains neuronal
636 excitability by reducing inwardly rectifying K+ conductance in layer V pyramidal neurons of mouse medial
637 prefrontal cortex. Front Mol Neurosci 15.

638 Staley KJ (2002) Diuretics as Antiepileptic Drugs: Should We Go with the Flow? Epilepsy Curr 2:39–40.

639 Stein V, Hermans-Borgmeyer I, Jentsch TJ, Hübner CA (2004) Expression of the KCl Cotransporter KCC2 Parallels Neuronal
640 Maturation and the Emergence of Low Intracellular Chloride. J Comp Neurol 468:57–64.

641 Stoppini L, Buchs PA, Muller D (1991) A simple method for organotypic cultures of nervous tissue. J Neurosci Methods
642 37:173–182.

643 Sulis Sato S, Artoni P, Landi S, Cozzolino O, Parra R, Pracucci E, Trovato F, Szczurkowska J, Luin S, Arosio D, Beltram F,
644 Cancedda L, Kaila K, Ratto GM (2017) Simultaneous two-photon imaging of intracellular chloride concentration
645 and pH in mouse pyramidal neurons in vivo. Proc Natl Acad Sci 114:E8770–E8779.

646 Taylor AL (2012) What we talk about when we talk about capacitance measured with the voltage-clamp step method. J
647 Comput Neurosci 32:167–175.

648 Temperini C, Cecchi A, Scozzafava A, Supuran CT (2009) Carbonic anhydrase inhibitors. Comparison of chlorthalidone,
649 indapamide, trichloromethiazide, and furosemide X-ray crystal structures in adducts with isozyme II, when
650 several water molecules make the difference. Bioorg Med Chem 17:1214–1221.

651 Thompson SM, Gahwiler BH (1989) Activity-dependent disinhibition. II. Effects of extracellular potassium, furosemide, and
652 membrane potential on E(Cl)- in hippocampal CA3 neurons. J Neurophysiol 61:512–523.

Tsien JZ, Chen DF, Gerber D, Tom C, Mercer EH, Anderson DJ, Mayford M, Kandel ER, Tonegawa S (1996) Subregion- and cell type-restricted gene knockout in mouse brain. Cell 87:1317–1326.

Tsukahara T, Masuhara M, Iwai H, Sonomura T, Sato T (2015) Repeated stress-induced expression pattern alterations of the hippocampal chloride transporters KCC2 and NKCC1 associated with behavioral abnormalities in female mice. Biochem Biophys Res Commun 465:145–151.

Tyzio R, Holmes GL, Ben-Ari Y, Khazipov R (2007) Timing of the developmental switch in GABAA mediated signaling from excitation to inhibition in CA3 rat hippocampus using gramicidin perforated patch and extracellular recordings. Epilepsia 48:96–105.

Uwera J, Nedergaard S, Andreasen M (2015) A novel mechanism for the anticonvulsant effect of furosemide in rat hippocampus in vitro. Brain Res 1625:1–8.

van Rheede JJ, Richards BA, Akerman CJ (2015) Sensory-Evoked Spiking Behavior Emerges via an Experience-Dependent Plasticity Mechanism. Neuron 87:1050–1062.

Viitanen T, Ruusuvuori E, Kaila K, Voipio J (2010) The K+-Cl- cotransporter KCC2 promotes GABAergic excitation in the mature rat hippocampus. J Physiol 588:1527–1540.

Wang BS, Feng L, Liu M, Liu X, Cang J (2013) Environmental Enrichment Rescues Binocular Matching of Orientation Preference in Mice that Have a Precocious Critical Period. Neuron 80:198–209.

Wang DD, Kriegstein AR (2008) GABA Regulates Excitatory Synapse Formation in the Neocortex via NMDA Receptor Activation. J Neurosci 28:5547–5558.

Wang DD, Kriegstein AR (2011) Blocking early GABA depolarization with bumetanide results in permanent alterations in cortical circuits and sensorimotor gating deficits. Cereb Cortex 21:574–587.

Wierenga CJ, Müllner FE, Rinke I, Keck T, Stein V, Bonhoeffer T (2010) Molecular and electrophysiological characterization of GFP-expressing ca1 interneurons in GAD65-GFP mice. PLoS ONE 5:1–11.

Wright R, Newey SE, Ilie A, Wefelmeyer W, Raimondo J V., Ginham R, Mcllhinney RAJ, Akerman CJ (2017) Neuronal Chloride Regulation via KCC2 Is Modulated through a $GABA_B$ Receptor Protein Complex. J Neurosci 37:5447–5462.

Yamada J, Okabe A, Toyoda H, Kilb W, Luhmann H, Fukuda A (2004) Cl− uptake promoting depolarizing GABA actions in immature rat neocortical neurones is mediated by NKCC1. J Physiol 557:829–841.

682 ## Figure legends

683 **Figure 1**. ***Furosemide acutely depolarizes the GABAergic driving force, but results in hyperpolarization after***
684 ***one week treatment.***

685 A, B) GABA reversal potential (E_{GABA}) (PT, p=0.33) and GABA Driving Force (GABA DF) (PT, p=0.19) values recorded
686 in CA1 pyramidal cells at DIV2 before and after acute application of furosemide. Data from 4 cells, 4 slices and 4
687 mice.

688 C, D) E_{GABA} (MW, p=0.004) and GABA DF (MW, p=0.002) values recorded in CA1 pyramidal cells at DIV21 before
689 and after acute application of furosemide. Data from 6 cells, 5 slices and 5 mice.

690 E, F) E_{GABA} (MW, p=0.001) and GABA DF (MW, p=0.005) recorded in CA1 pyramidal cells at DIV9 in control (CTL)
691 and furosemide-treated slices. Data from 7-9 cells, 5-8 slices and 4-5 mice per group.

692 G) Average SClm FRET ratios in CTL and furosemide-treated slice cultures (UT, p=0.75). Data from 10-14 slices
693 and 6-10 mice per group.

694 H) Cumulative distribution of FRET ratios in individual cells in CTL and furosemide -treated cultures. (KS, p=0.23).
695 Data from 15 randomly selected cells per slice.

696 I) Western blots of NKCC1, KCC2 and S940-pKCC2 (pKCC2) protein levels in CTL and furosemide-treated slice
697 cultures. Tubulin (Tub) was used as loading control.

698 J) Summary of data for NKCC1, KCC2 and for s940-pKCC2 (pKCC2) protein levels. Values were normalized to the
699 protein level in CTL cultures (NKCC1: MW, p>0.99; KCC2: MW, p=0.70; pKCC2: MW, p=0.48). Data from 3-5
700 experiments and 3 mice per group.

701 K) Confocal images of NeuN and KCC2 staining in CTL and furosemide-treated cultures. Yellow lines indicate the
702 outlines of individual cells. Scale bar: 10 µm.

703 L) Total KCC2 levels (UT, p=0.55) and KCC2 levels in membrane (UT, p=0.37) in CTL and furosemide-treated
704 cultures. Each datapoint represents the mean KCC2 intensity of all neurons in one image. Data from 8-17 images,
705 4-8 slices and 3 mice per group.

706

707 **Figure 2.** ***Furosemide does not affect inhibitory transmission at DIV9.***

708 A-E) sIPSC frequency (MW, p=0.084), amplitude (UT, p=0.83), risetime (MW, p=0.80) and decay tau (MW,
709 p=0.57) and membrane capacitance (Cm) (UT, p=0.63) in control (CTL) and furosemide-treated slice cultures at
710 DIV9. Data from 14-17 cells, 9 slices and 9 mice per group.

711 F-I) sIPSC frequency after ACSF wash in as a control CTL (WSR, p=0.008) and furosemide-treated (WSR, p=0.002)
712 slice cultures at DIV9. sIPSC frequency after TTX wash in of in CTL (WSR, p=0.80) and furosemide-treated WSR,
713 p=0.002) slice cultures at DIV9. Data from 8-15 cells, 8-15 slices and 7-10 mice per group.

714 J) Change in sIPSC frequency after ACSF wash in as a control, versus after wash in of TTX, K252a, AM251 and
715 agatoxin-IVA (aga) to block neuronal activity, BDNF, endocannabinoids and P/Q calcium channels respectively in
716 control and furosemide-treated slices at DIV9 (2W ANOVA, treatment p=0.18, blocker p=0.002; SMC, control
717 versus TTX, p=0.95; control versus K252a, p=0.020; control versus AM251, p=0.99; control versus agatoxin-IVA
718 (aga), p=0.82). Data from 7-15 cells, 7-15 slices and 4-10 mice per group.

719 **Figure 3.** ***Furosemide increases inhibitory transmission at DIV21.***

720 A,B) GABA reversal potential (E_{GABA}) (MW, p=0.56) and GABA Driving Force (GABA DF) (MW, p=0.76) in control
721 (CTL) and furosemide-treated slice cultures at DIV21. Data from 9-13 cells, 9 slices and 9 mice per group.

722 C) sIPSC recording from CA1 pyramidal cells in CTL and furosemide-treated organotypic cultures at DIV21. sIPSCs
723 are indicated with *.

724 D-G) sIPSC frequency (UT, p=0.10), amplitude (UT, p=0.034), risetime (UT, p=0.54) and decay tau (UT, p=0.34) in
725 CTL and furosemide-treated slice cultures at DIV21.

726 I) Membrane capacitance (Cm) of CA1 pyramidal cells in CTL and furosemide-treated slice cultures at DIV21 (UT,
727 p=0.035).

728 I) mIPSC recording from CA1 pyramidal cells in control and furosemide-treated organotypic cultures at DIV21.
729 mIPSCs are indicated with *.

730 J-M) mIPSC frequency (UT, p=0.0002), amplitude (UT, p=0.34), risetime (MW, p=0.73) and decay tau (UT, p=0.06)
731 in CTL and furosemide-treated organotypic cultures at DIV21.

732 N) Membrane capacitance (Cm) of CA1 pyramidal cells in the presence of TTX in CTL and furosemide-treated
733 slice cultures at DIV21 (UT, p=0.35). Data in D-H from 11-12 cells, 5-6 slices and 3-5 mice per group; data in J-N
734 from 12-13 cells, 5 slices and 4 mice per group.

735

736 **Figure 4.** ***Furosemide does not affect inhibitory synapses at DIV9.***

737 A,B) VGAT, PV and CB1R immunofluorescence in the CA1 *stratum Pyramidale* (*sPyr)* and *stratum Radiatum*
738 (*sRad)* of control (CTL) and furosemide-treated organotypic cultures at DIV9. Scale bar=10 µm.

739 C,D) The density (UT, p=0.50) and size (UT, p=0.47) of VGAT puncta in the *sPyr* of CTL and furosemide-treated
740 organotypic cultures at DIV9.

741 E,F) The density (UT, p=0.59) and size (UT, p=0.46) of VGAT puncta in *sRad* of CTL and furosemide-treated
742 organotypic cultures at DIV9.

743 G,H) The density of CB1R-positive VGAT puncta (UT, p=0.43) and PV positive VGAT puncta (UT, p=0.82) in *sPyr*
744 of CTL and furosemide-treated organotypic cultures at DIV9.

745 I) The density of CB1R-positive VGAT puncta (UT, p=0.68) in *sRad* of CTL and furosemide-treated organotypic
746 cultures at DIV9.

747 Data in C-I from 11-12 images, 6 slices and 2 mice per group.

748

749 **Figure 5.** ***Furosemide increases the number of VGAT puncta at DIV21 in sRad.***

750 A,B) VGAT, PV and CB1R immunofluorescence in the CA1 *stratum Pyramidale* (*sPyr)* and *stratum Radiatum*
751 (*sRad)* of control (CTL) and furosemide-treated organotypic cultures at DIV21. Scale bar=10 µm.

752 C,D) The density (UT, p=0.09) and size (UT, p=0.14) of VGAT puncta in *sPyr* of CTL and furosemide-treated
753 organotypic cultures at DIV21. Data from 16 images, 8 slices and 3 mice per group.

754 E,F) The density (MW, p=0.019) and size (MW, p=0.015) of VGAT puncta in *SRad* of CTL and furosemide-treated
755 organotypic cultures at DIV21. Data from 13 images, 7 slices and 3 mice per group.

G,H) The density of CB1R (UT, p=0.11) and PV positive VGAT puncta (UT, p=0.89) in *sPyr* of CTL and furosemide-treated organotypic cultures at DIV21. Data from 16 images, 8 slices and 3 mice per group.

I) The density of CB1R-positive VGAT puncta (MW, p=0.30) in *SRad* of CTL and furosemide-treated organotypic cultures at DIV21. Data from 13 images, 7 slices and 3 mice per group.

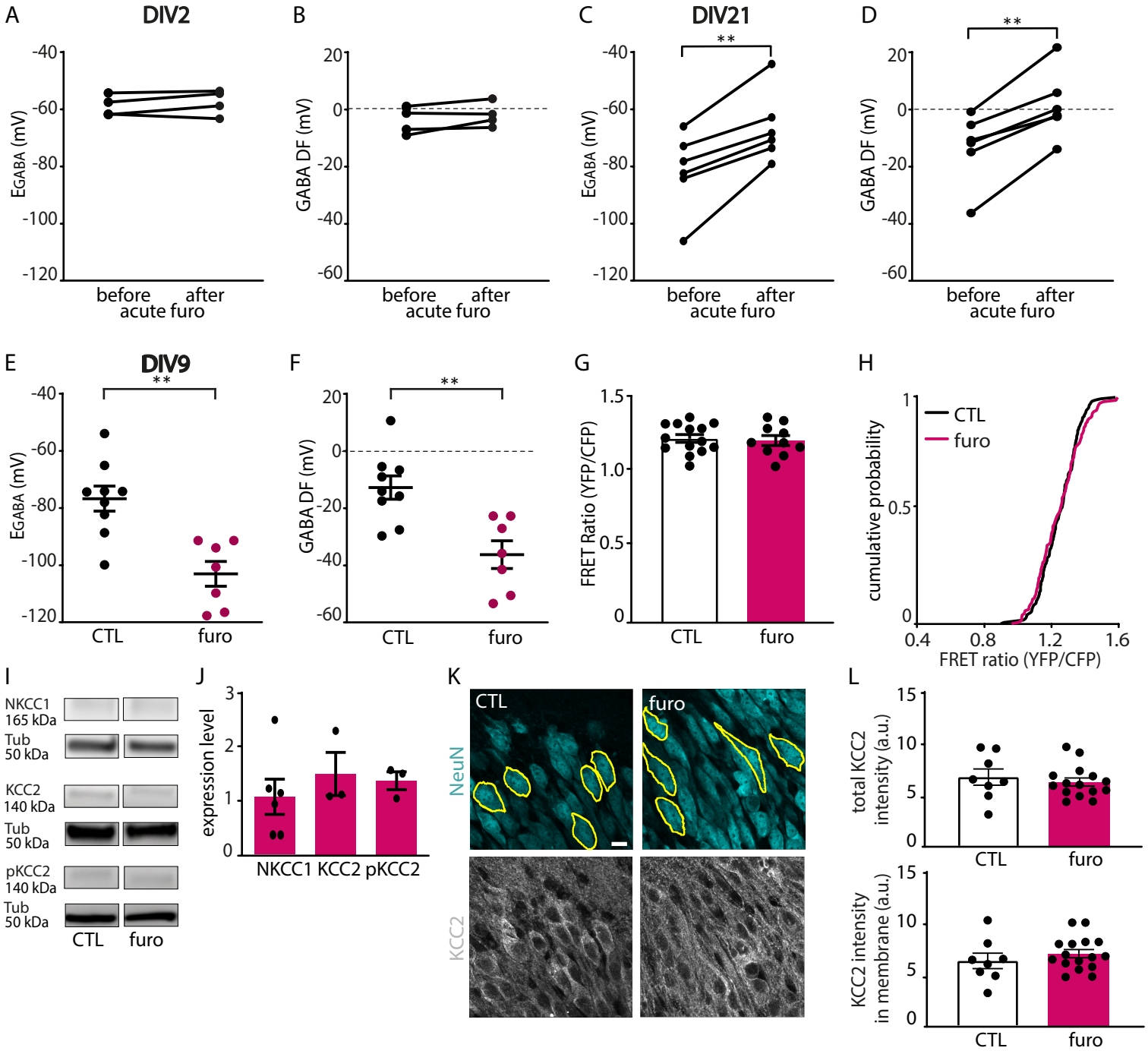

Peerboom et al. - Figure 1

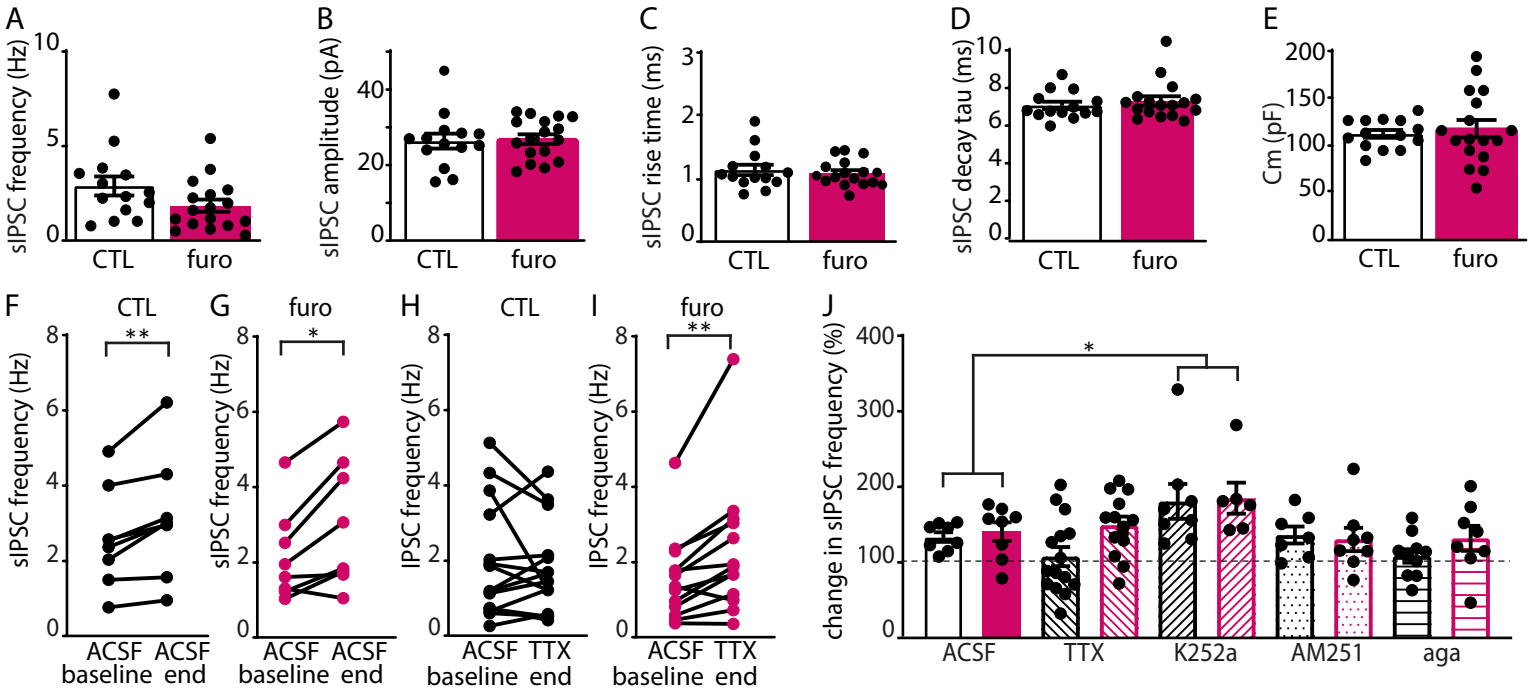

Peerboom et al. - Figure 2

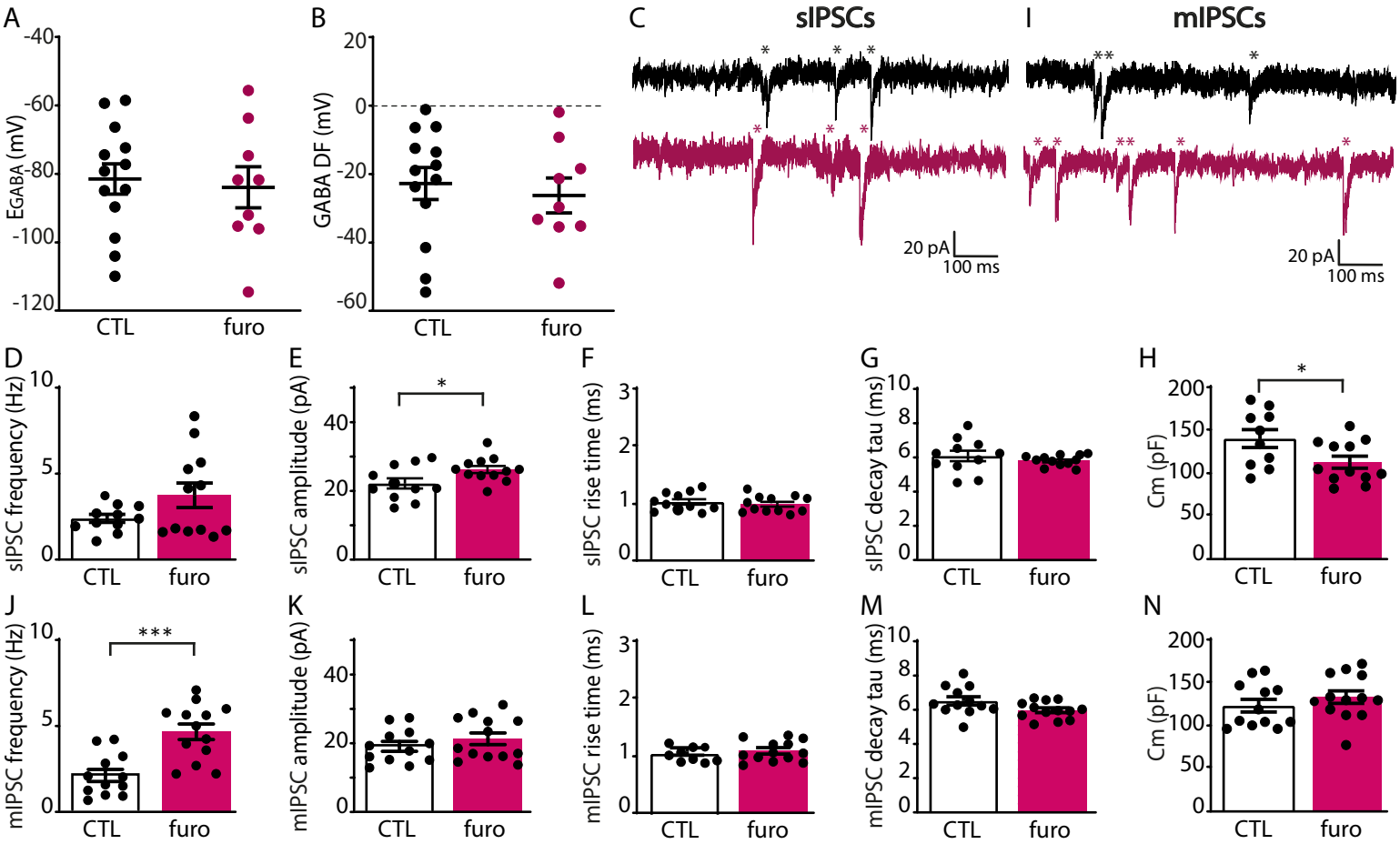

Peerboom et al. - Figure 3

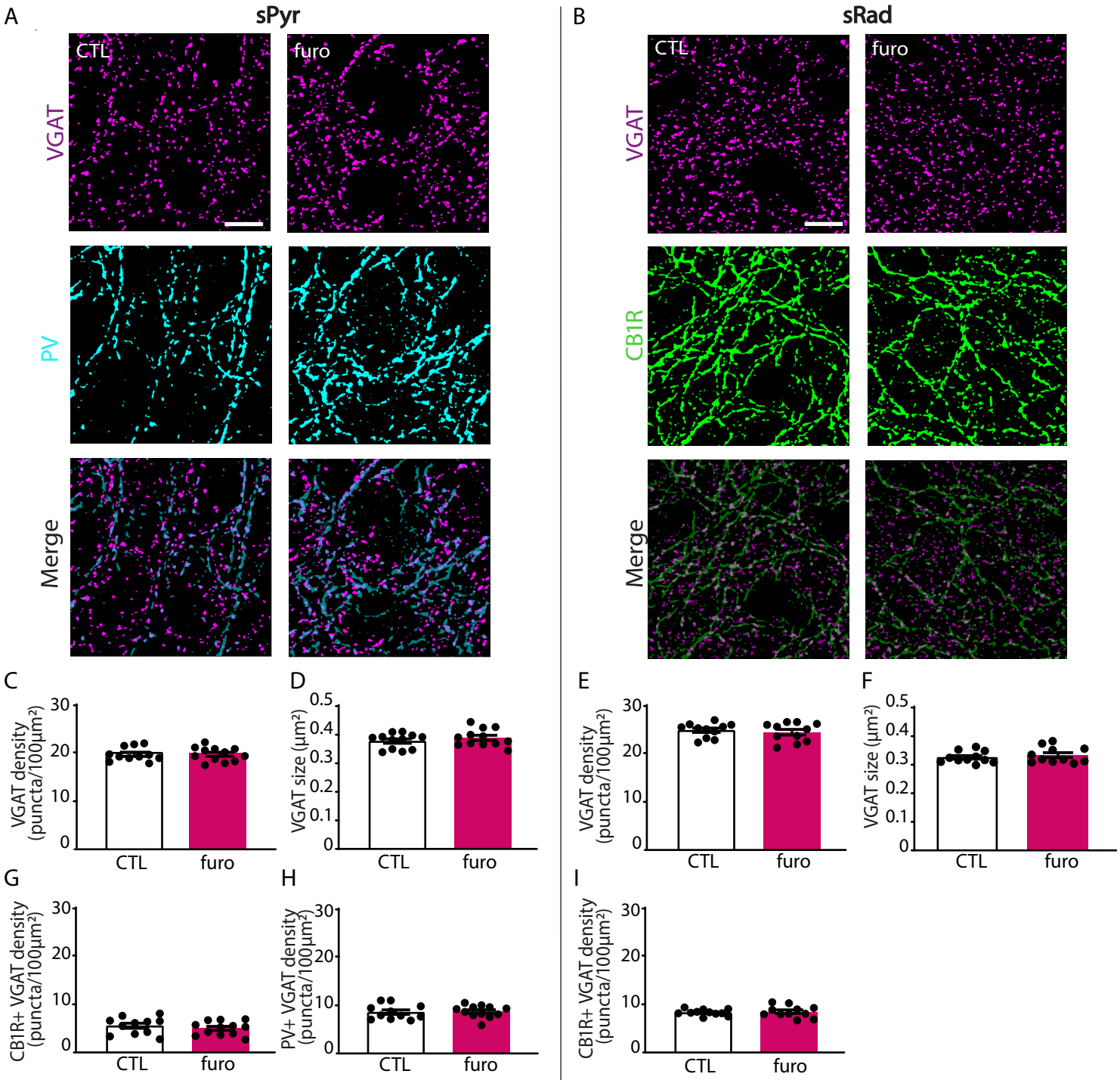

Peerboom et al. - Figure 4

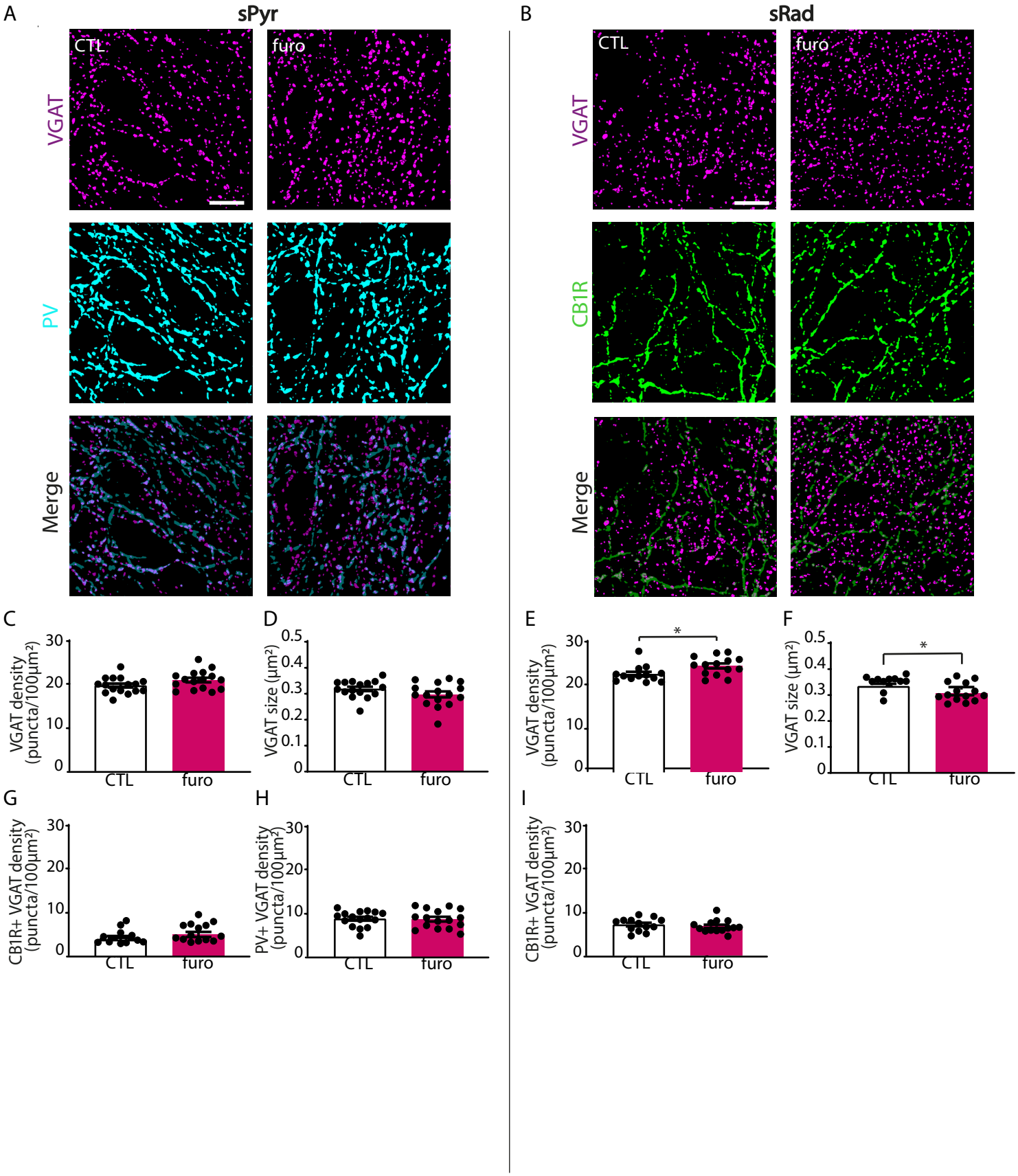

Peerboom et al. - Figure 5